A simple RANS closure for wind-farms under neutral atmospheric conditions Preliminary findings

Jigjid, Kherlen; Dwight, Richard; Allaerts, Dries; Steiner, Julia

DOI
10.1088/1742-6596/2767/9/092104

Publication date
2024

Document Version
Final published version

Published in
Journal of Physics: Conference Series

A simple RANS closure for wind-farms under neutral atmospheric conditions: Preliminary findings

Journal of Physics: Conference Series **2767** (2024) 092104 doi:10.1088/1742-6596/2767/9/092104

A simple RANS closure for wind-farms under neutral atmospheric conditions: Preliminary findings

Kherlen Jigjid, Richard Dwight, Dries Allaerts, Julia Steiner

Faculty of Aerospace Engineering, Delft University of Technology, Kluyverweg 1, 2629 HS Delft, NL

E-mail: k.jigjid@tudelft.nl

Abstract. Accurately predicting wind turbine wake effects is essential for optimizing wind-farm performance and minimizing maintenance costs. This study explores the applicability of the Sparse Regression of Turbulent Stress Anisotropy (SpaRTA) framework to develop a simple yet robust Reynolds-averaged Navier-Stokes (RANS) model for wake prediction in wind energy contexts. The framework introduces two correction terms into two-equation models, with $k-\varepsilon$ model being utilized in the current study. One correction term resembles the residual of the Turbulent Kinetic Energy (TKE) equation, and the other corrects the deviatoric part of the Reynolds Stress Tensor (RST). The terms are calculated from high-fidelity measurement or simulation data, and symbolic regression is used to determine the model for these terms.

In this study, Large Eddy Simulation (LES) data from a single turbine is used as the training dataset, and a sample pre-selection process is employed to discover a correction model efficiently. The derived model incorporates two terms based on Pope's basis tensors and their invariants. The expression of the obtained model shows that it functions as a modification to the constant C_μ in the $k-\varepsilon$ model. The model is evaluated by comparing its predicted velocity and TKE fields with the LES data used for the training. The model showed satisfactory performance in predicting both fields. Additionally, its generalizability is evaluated by testing it against a more complex six-turbine unseen case. The results indicate that the model effectively captures the velocity field and power output, but it tends to overpredict TKE, especially in the wake region.

1. Introduction

The accurate prediction of wind turbine wake effects is crucial for estimating wind-farm yields, optimizing design, and ensuring efficient land utilization while reducing maintenance costs. This is particularly pronounced in larger and denser wind-farms, where wake interactions occur frequently, exerting a substantial influence on overall performance. In large scale offshore wind-farms, wake losses can account for a 10-20% reduction in total power output [1]. Additionally, wake-induced turbulence can result in complex flow patterns that cause structural vibrations in downstream wind turbines, leading to premature fatigue and increased maintenance costs [2]. Consequently, there's a clear demand for an efficient and precise wake prediction method.

Various methods are available for predicting wakes, including analytical models commonly employed in industry and Computational Fluid Dynamics (CFD) methods primarily used in academic research. While analytical models are cost-effective, their accuracy diminishes in dense wind-farms with cumulative effect of wakes [3]. In such scenarios, numerical models become more suitable. Among these, Large Eddy Simulation (LES) can yield precise predictions but demands between 10^3 and 10^4 CPU hours, making it challenging for industrial applications

[4]. Given these limitations, Reynolds-averaged Navier-Stokes (RANS) models offers a better compromise between accuracy and cost. Nevertheless, their effectiveness relies on the selection of the appropriate closure model and its parameters [5].

A recent development in enhancing RANS models involves the data-driven framework Sparse Regression of Turbulent Stress Anisotropy (SpaRTA) [6]. This approach introduces two correction terms into standard two-equation models. The terms are derived from high-fidelity data, such as LES or measurement data. These terms are then modeled utilizing sparse regression, yielding simple mathematical expressions and mitigating the 'black-boxification' issue commonly associated with neural network-based models. The effectiveness of the SpaRTA framework has been demonstrated in various applications, including wind-tunnel scaled wind-farms [7], and three-dimensional bluff bodies [8].

Considering the above, this study utilizes the SpaRTA framework in a full-scale wind-farm simulation, aiming to study its applicability in wind energy contexts. The primary objective is to develop a data-driven RANS model that balances simplicity, accuracy and generalizability for predicting wakes and wind-farm power production. To achieve this, a model is derived by using LES data of a single turbine, serving as a simpler case. A subset of the data is utilized as the training sample, filtered according to the specified thresholds. This enhances the efficiency of the model search process and increases the chance of discovering a simpler model. The performance of the discovered model is assessed by predicting velocity and Turbulent Kinetic Energy (TKE) fields. Furthermore, to evaluate its generalizability, the model is tested against an unseen LES data case involving six turbines, which includes wind turbine power output prediction as well.

The remainder of this paper is organized into three sections. In Section 2, the SpaRTA framework and its implementation for the current study are detailed, along with the description of the precursor simulations, the dataset used, and the sampling method. Section 3 includes the outcomes of the precursor simulations, an explanation of the obtained model, predictions for TKE and velocity fields, and power output predictions by the model. Lastly, Section 4 provides a summary of the research results, accompanied by suggestions for future research directions.

2. Methodology

2.1. SpaRTA framework

To implement the SpaRTA framework, the governing equations must be formulated based on two-equation models. In the present research, the $k-\varepsilon$ model is selected as the baseline model for its simplicity and widespread application in the field, and is often used as the base model for different models, including the $k-\varepsilon-f_P$ model [9]. For obtaining the governing equations, two additional terms are introduced into the base model. The terms include R, the residual of the k-equation that corrects all compatibility errors between the model and the LES data, and b_{ij}^{Δ}, which corrects the deviatoric part of the Reynolds Stress Tensor (RST). Incorporating the two correction terms into the equations of the standard $k-\varepsilon$ model, we obtain:

$$D_t U_i = -\frac{1}{\rho}\partial_i(P+\frac{2\rho k}{3}) + \partial_j\left(2\nu S_{ij} + 2\nu_t S_{ij} - 2k b_{ij}^{\Delta}\right) + f_x + f_T, \tag{1}$$

$$D_t k = P_k + P_k^{\Delta} - \varepsilon + \partial_j\left[\left(\nu + \frac{\nu_t}{\sigma_k}\right)\partial_j k\right] + R, \tag{2}$$

$$D_t \varepsilon = C_{\varepsilon 1}(P_k + P_k^{\Delta} + R)\frac{\varepsilon}{k} - C_{\varepsilon 2}\frac{\varepsilon^2}{k} + \partial_j\left[\left(\nu + \frac{\nu_t}{\sigma_\varepsilon}\right)\partial_j \varepsilon\right], \tag{3}$$

$$P_k + P_k^{\Delta} = -2k\left(b_{ij} + b_{ij}^{\Delta}\right)\partial_j U_i = -2k\left(-\frac{\nu_t}{k}S_{ij} + b_{ij}^{\Delta}\right)\partial_j U_i, \tag{4}$$

where, t, U_i, ρ, P, ν, ν_t, S_{ij}, f_x, f_T represent time, mean velocity components, fluid density, pressure, kinematic viscosity, eddy viscosity (defined as $\nu_t = C_\mu k^2/\varepsilon$), mean strain rate tensor,

Atmospheric Boundary Layer (ABL) driving force and turbine force respectively. Additionally, k represents the TKE, with ε denoting its destruction rate and P_k indicating its production rate. Moreover, b_{ij} represents the deviatoric part of the RST. The parameters C_μ, $C_{\varepsilon 1}$, $C_{\varepsilon 2}$, σ_ε and σ_k in (2)-(4) are typically determined from existing literature.

With the derived equations, the SpaRTA framework operates in the following manner. Firstly, the correction terms are derived from high-fidelity data, which in this study comprises time-averaged LES data. The terms are calculated by imposing U, k and RST τ_{ij} field data into (2)-(4), to solve for R and b_{ij}^{Δ}. This step is called "frozen approach" in the framework. Subsequently, the obtained terms, called "frozen correction terms", are integrated into a RANS simulation for validation in the "propagation RANS" step. If the results closely match to the high-fidelity data, these terms will be assigned as the target for the "model discovery" phase, which employs symbolic regression, as the last step of the framework. This process begins by creating a function library. The library comprising terms derived from Pope's basis tensors and invariants [10], along with their combinations. Once the library is prepared, a coefficient vector, which incorporates the significance of each library term, is optimized to minimize the error between the prediction and the target. This is achieved through sparse-regression with elastic net regularization, resulting in many coefficients being forced to zero. The resulting model is a linear combination of the remaining terms from the function library and can be directly incorporated into the $k-\varepsilon$ model. The model could be expressed as $R = \Theta_{(R)} C_{(R)}$ and $b_{ij}^{\Delta} = \Theta_{(b_{ij}^{\Delta})} C_{(b_{ij}^{\Delta})}$. Here, Θ and C represent the vector formulation of the function library and coefficients vector, respectively.

In the present study, during the implementation of the framework, the correction terms are divided into two components, as done similarly in [7]. One component is dedicated to inlet profile corrections, referred to as ABL correction, while the other focuses on wake correction. This separation can be written as follows:

$$b_{ij}^{\Delta} = b_{ij}^{\Delta,\mathrm{ABL}} + b_{ij}^{\Delta,\mathrm{Wake}}, \qquad R = R^{\mathrm{ABL}} + R^{\mathrm{Wake}}. \tag{5}$$

Generally, the inlet profile in RANS simulations cannot replicate that of LES because they are computed using distinct governing equations and models in the simulations. Consequently, in the "frozen approach", the correction terms may include not only wake-related but also inlet profile-related corrections. This is not desirable in model development, and it is preferable to handle wake and inlet profile corrections separately. By doing so, model that focuses solely on correcting for wake can be obtained, avoiding any dependence on the inlet profile.

In the current study, four types of RANS simulations were conducted, each utilizing a distinct combination of correction terms as listed in Tab. 1. The full propagation RANS applies all the frozen correction terms, while the frozen-b_{ij}^{Δ} propagation and model-b_{ij}^{Δ} RANS similarly employ all the correction terms except for R^{Wake}. However, the model-b_{ij}^{Δ} RANS utilizes model-derived $b_{ij}^{\Delta,\mathrm{Wake}}$. In contrast, the baseline RANS applies no corrections. During the study, it became clear that the improvement is mainly coming from $b_{ij}^{\Delta,\mathrm{Wake}}$ instead of R^{Wake}, which will be presented later in Sec. 3.2. Regarding this, the study focus on discovering a model for the $b_{ij}^{\Delta,\mathrm{Wake}}$, with frozen-$b_{ij}^{\Delta}$ propagation RANS serving as the prediction of the best possible model.

Table 1: Correction terms corresponding to each RANS simulation.

RANS simulation type	$R =$	$b_{ij}^{\Delta} =$
Full propagation	frozen-R^{ABL} + frozen-R^{Wake}	frozen-$b_{ij}^{\Delta,\mathrm{ABL}}$ + frozen-$b_{ij}^{\Delta,\mathrm{Wake}}$
Frozen-b_{ij}^{Δ} propagation	frozen-R^{ABL}	frozen-$b_{ij}^{\Delta,\mathrm{ABL}}$ + frozen-$b_{ij}^{\Delta,\mathrm{Wake}}$
Model-b_{ij}^{Δ}	frozen-R^{ABL}	frozen-$b_{ij}^{\Delta,\mathrm{ABL}}$ + model-$b_{ij}^{\Delta,\mathrm{Wake}}$
Baseline	None	None

2.2. Precursor simulations

To conduct full-scale wind-farm RANS, precursor simulations are essential to acquire the inlet profile and simulation parameters for the baseline and propagation RANS simulations. Moreover, it is also required for obtaining $b_{ij}^{\Delta,\mathrm{ABL}}$ and R^{ABL} for the propagation RANS simulations.

For the both baseline and propagation RANS simulations, the reference profiles are extracted from corresponding cases of LES data, which are presented in Sec. 2.3. The profiles consist of U and k fields, obtained by averaging across the lateral direction y of the profile at the streamwise position $x = 200$ m. It was observed that the inlet profile evolves until $x = 200$ m, with negligible evolution thereafter until reaching the first turbine at $x = 400$ m. Based on this observation, the location of the reference profile is determined.

To align the RANS inlet profile with that of LES, two parameters, surface roughness length z_0 and ABL driving force f_x, undergo optimization. A rough wall Boundary Condition (BC) is implemented at the wall to match the LES setup, with z_0 representing the degree of roughness. It exerts significant influence on the first cell in the vertical direction, thereby impacting the entire profile. Meanwhile, the second parameter, f_x, appears as a body forcing term within the momentum equations, driving the wind profile through the simulation domain. The optimization process employs the Nelder-Mead algorithm [11]. The objective function is based on the combined error of Mean Absolute Error (MAE) and Root Mean Squared Error (RMSE) between the LES and RANS U and k profiles within the turbine height region. The obtained values of the two parameters, z_0 and f_x, which yield the desired inlet profile closely aligned with the LES data, are then utilized in full-scale RANS simulations.

2.3. LES dataset

In this study, LES data of a wind-farm under a truly neutral ABL, characterized by a pressure-driven boundary layer without Coriolis and temperature effects, is utilized. The data is sourced from [5], which is generated by in-house pseudo spectral code, that is also used in [12].

The dataset comprises two distinct cases, both featuring a domain size of 4800 m (480 cells) in the streamwise direction x, 800 m (160 cells) in the lateral direction y, and 355 m (71 cells) in the vertical direction z. The domain is discretized uniformly in each direction, resulting in a total cell count of approximately 5.5 million cells for each case. The inlet turbulence intensity at the hub height (defined as $I_h = \sqrt{2k/3}/U_h$, with $U_h = 8$ m/s representing the mean velocity at the hub height) is consistently 5.8% for the both cases. The cases differ in the configuration of wind turbine placements, as illustrated in Fig. 1. In case 1T (a), there is a single turbine. Conversely, case 6T7D (b) features two columns of six wind turbines, with a distance of $7D$ between each turbine, where D denotes a turbine diameter. In the figure, all axes are normalized by D, following the standard practice in the wind industry.

A non-rotational Actuator Disk (AD) method is employed to model the wind turbines for all the simulations, following the approach outlined in [13]. The disk-based thrust coefficient C_t' is

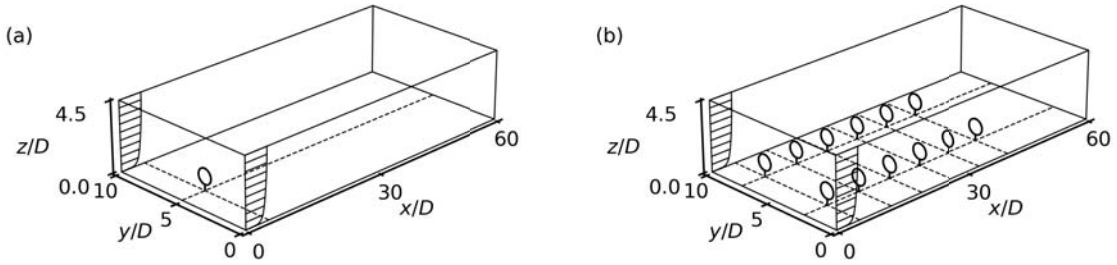

Figure 1: Computational domain and wind turbine configurations of LES data for cases (a) 1T and (b) 6T7D. Length along each axis are normalized with D.

set to $C_t' = 4a/(1-a)$, where a represents the induction factor. In this study, a is fixed at 0.25, resulting in $C_t' = 4/3$, consistent with [5]. The turbine parameters remain consistent across the both cases, with a $D = 80$ m and a turbine hub height z_h set at 70 m. The turbine force is calculated based on the disk-averaged velocity and uniformly distributed over the disk regions, with a Gaussian filter subsequently smoothing the distribution of these forces throughout the computational domain in $y - z$ plane. The standard deviation σ for the Gaussian filter size is set at approximately 8 meters. For more details about the AD method, please refer to [13].

The LES data used in this research underwent pre-processing procedures. The data are time-averaged to ensure comparability with the RANS solutions. In the case of 6T7D, the fields were spatially averaged with respect to the $y = 5D$ plane to improve the statistical representation of the data. This averaging process involved extracting domains within the ranges of $0 \leq y \leq 5D$ and $5D \leq y \leq 10D$, followed by the computation of field averages. However, in the case of 1T, spatial averaging was not performed. Instead, a domain of $2.5D \leq y \leq 7.5D$ was extracted to align with the domain size of the other case. Moreover, there is a fringe zone in the downstream of the domain, thus to avoid its effect, $55D < x$ region is omitted from any analysis.

2.4. Selection of training samples

In the model discovery phase of the SpaRTA framework, the 1T case is utilized. This decision leverages the inherent simplicity of the 1T case, establishing it as an ideal scenario for model development. If the model, derived from this simpler case, can accurately predict for the more complex 6T7D case, it implies that the model is capable of capturing the general physical patterns present in both scenarios. Furthermore, the accuracy of these predictions provides some assurance of the model's generalizability.

Furthermore, the selection of samples from the 1T case was conducted intentionally. Instead of covering the entire domain, which includes less relevant areas like the free stream or the boundary regions, a more focused set of samples located near the turbine wake was selected. This process involved setting a threshold for the $P_k^{\Delta,\mathrm{Wake}}$ field, which is a k production term that resulted from frozen approach-derived $b_{ij}^{\Delta,\mathrm{Wake}}$. Samples were chosen where $P_k^{\Delta,\mathrm{Wake}}$ exceeds 0.001 or falls below -0.001, as depicted by the isolines in Fig. 2, focusing on substantial non-zero $P_k^{\Delta,\mathrm{Wake}}$ values. As shown in the figure, most of the samples are from the wake region, with some collected from the wall regions. However, samples that have boundaries with walls are excluded due to their reliance on wall function. Regarding above, the thresholds are deemed suitable for the case 1T, nevertheless, the values can be chosen differently for different cases.

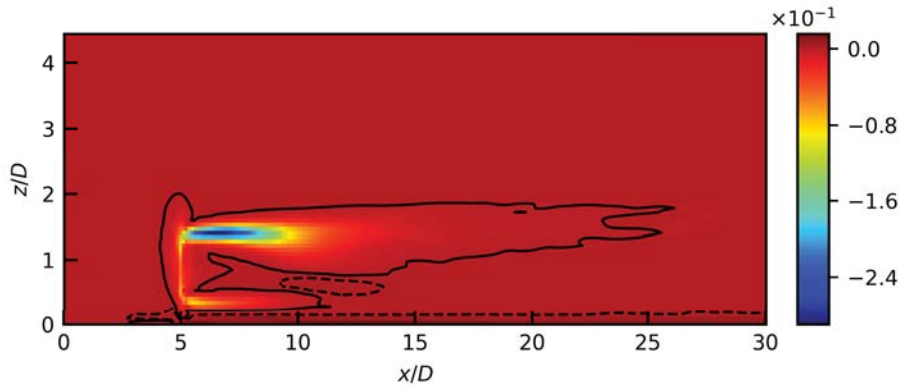

Figure 2: The $x - z$ plane of the $P_k^{\Delta,\mathrm{Wake}}$ field at $y = 5.0D$ for the full propagation RANS. The isolines represent -0.001 (solid) and 0.001 (dashed) lines.

Table 2: Model and simulation parameters used for the baseline and propagation RANS. The model parameters are based on the standard $k-\varepsilon$ model [14].

	RANS parameters:					Simulation parameters:	
Simulation type	C_μ	$C_{\varepsilon 1}$	$C_{\varepsilon 2}$	σ_ε	σ_k	z_0 [m]	f_x [m/s^2]
Baseline	0.09	1.42	1.92	1.00	1.30	0.0117	0.000339
Propagation	0.09	1.42	1.92	1.00	1.30	0.00296	0.000286

3. Results

3.1. Precursor simulation results

The standard $k-\varepsilon$ model [14] is considered as the baseline RANS model for the current study, and thus, the precursor simulations also implement the same model. The parameters for the standard $k-\varepsilon$ model used in baseline and propagation RANS are listed in Tab. 2, with both cases utilizing the same set of parameters. Similarly, simulation parameters z_0 and f_x that are obtained from the precursor simulations mentioned in Sec. 2.2 are also tabulated.

In Figure 3, a comparison of the inlet profiles between LES and RANS simulations is presented. Profiles comparison between LES and RANS results indicates good agreement. However, in the baseline RANS, a significant difference appears in the k profile near the wall. In contrast, the propagation RANS effectively corrects this deficiency in the near-wall region observed in the baseline RANS, and improvements are observed in other parts of the profile as well. These results highlight the accuracy of the ABL correction terms. However, there is still a minor mismatches near the wall for the propagation RANS. It is common that LES overestimates the peak of k near the wall, resulting in unreliable values in that region. Nonetheless, achieving an exact match in the near-wall region is not the primary concern and does not impact the outcome of the study, since the main focus of this research is predicting wake behavior in the turbine region. Consequently, the obtained correction terms $b_{ij}^{\Delta,\mathrm{ABL}}$ and R^{ABL} are implemented for all propagation RANS, along with the corresponding inlet profiles.

3.2. Full-scale simulation results

Incorporating the inlet profiles, simulation parameters, and inlet profile corrections obtained in Sec. 3.1, the four types of full-scale RANS simulations are conducted, with the results presented in this section. In Figure 4, a comparison of the U_x and k fields at the mid $x-z$ plane is illustrated for case 1T.

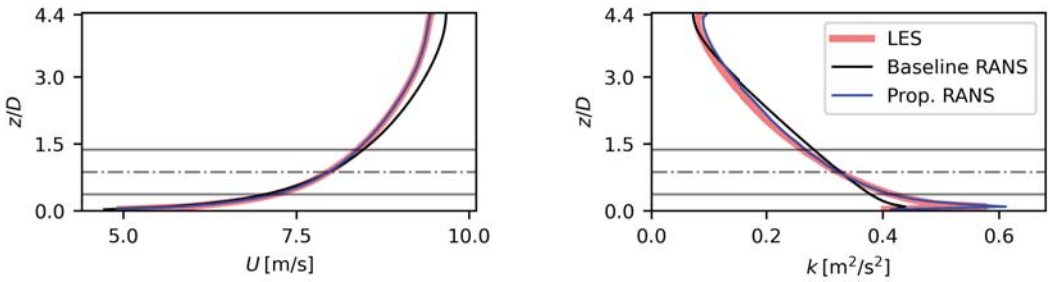

Figure 3: Comparison of inlet profiles in the z direction for U_x and k between LES data (red solid line), baseline RANS (black line) and propagation RANS (blue line). The profiles are plotted against the normalized vertical coordinate z/D. Turbine borders are indicated by the gray solid lines, and the turbine hub-height is by the dot-dashed line.

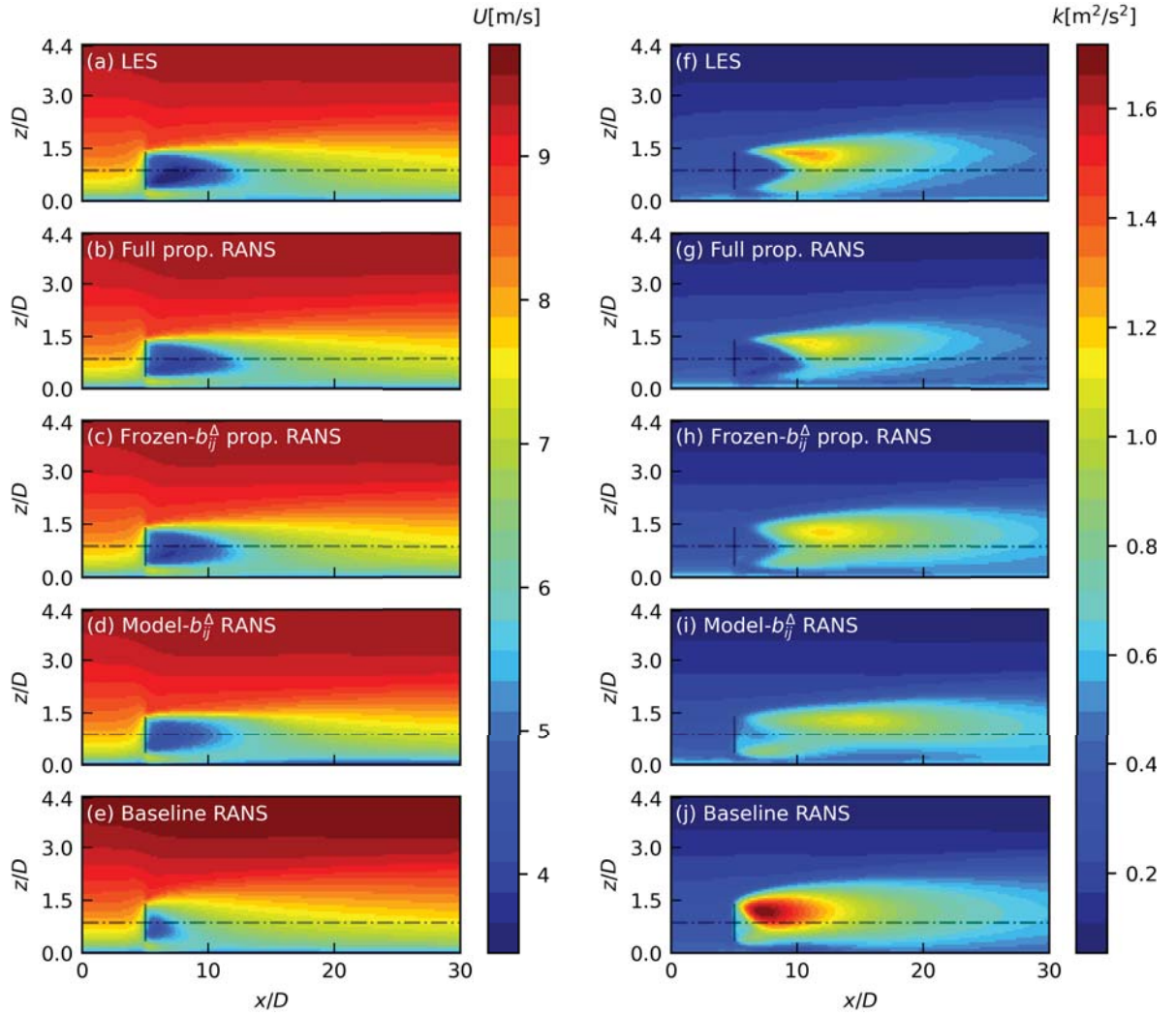

Figure 4: Comparison of $x-z$ planes of U_x (left column) and k (right column) fields at $y = 2.5D$ for 1T case simulations. Top to bottom, LES (a, f), full propagation RANS (b, g), frozen-b_{ij}^{Δ} propagation RANS (c, h), model-b_{ij}^{Δ} RANS (d, i), and baseline RANS (e, j) fields are shown, respectively. Dark rectangles represent the ADs, and dash-dotted lines indicate the hub heights.

Upon comparing the U_x and k fields from full propagation RANS (b, g) with those of LES (a, f), it becomes apparent that the results are closely aligned across most regions. This validates the accountability of the frozen correction terms, and supports the decision to set the terms as the target for the model discovery phase.

Although utilizing all the correction terms improve the accuracy significantly, the primary source of improvement originates from the correction of turbulence anisotropy via $b_{ij}^{\Delta,\mathrm{Wake}}$ as mentioned in Sec. 2.1. It can be seen when comparing figures (c, h) – which are generated with frozen-b_{ij}^{Δ} propagation RANS – to the figures above them (b, g). While there are slight differences in the distribution of the k field within the wake region, the peak position remains consistent. As for the U_x fields, they exhibit nearly identical behavior. Consequently, the focus of the model discovery process in this study is exclusively on $b_{ij}^{\Delta,\mathrm{Wake}}$.

In terms of the predictions by the model-b_{ij}^{Δ} RANS, the distribution of k (i) closely resembles that of frozen-b_{ij}^{Δ} propagation RANS (h), though its peak is shifted slightly downstream.

Regarding the U_x field (d), it is very much the same as (c). The algebraic expression of the model that is being implemented is:

$$\text{Model-}b_{ij}^{\Delta,\text{Wake}} = \frac{1}{68}\left[1 + 4.55 \cdot \tanh\left(\frac{(I_1/\omega^2)}{81.097}\right)\right](T_{ij}^{(1)}/\omega), \tag{6}$$

where $T_{ij}^{(1)} = S_{ij}$ represents the first tensor of the Pope's basis tensors, and $I_1 = S_{ij}S_{ij}$ denotes the first invariant, as defined in [10]. Regarding the model having $T_{ij}^{(1)}$ outside the largest bracket, it can be reformulated in terms of a C_μ modification. Specifically, the terms $2\nu_t S_{ij}$ and $2kb_{ij}^{\Delta}$ in (1) can be combined into a single equation, $2\nu_t f_P S_{ij}$, through the introduction of f_P, as similar in [15]. Subsequently, the term f_P can be expressed as,

$$f_P = 1 - \frac{1}{68 \cdot C_\mu}\left[1 + 4.55 \cdot \tanh\left(\frac{(I_1/\omega^2)}{81.097}\right)\right] \tag{7}$$

This formulation suggests that the model acts as a C_μ correction, locally adjusting the original C_μ value based on the local I_1/ω^2 value. Furthermore, when $C_\mu = 0.09$, the values of f_P ranges between 0.093 and 0.83, considering the "tanh" function's range from 0 to 1 with $I_1 \geq 0$ condition. This means the model reduces C_μ value across the entire domain and further decreases the value in regions with higher velocity gradient, where the wake is prominent.

The last row of the Fig. 4 (e, j) highlights the limitations of the $k-\varepsilon$ model, particularly in its prediction of a faster wake recovery for U_x, primarily due to its overestimation of k in the near the turbine region, aligning with the study [5]. It's important to note that the authors are aware that the $k-\varepsilon$ model may not be the most suitable choice for the current simulation cases. Nevertheless, it is implemented to demonstrate the correction terms' ability to improve predictions, even when applied to the simplest model.

To demonstrate the capability of the model, we applied it to an unseen case (of greater complexity than the training case), with a row of 6 turbines at a $7D$ spacing (6T7D). The results are shown in Fig. 5. The ordering of the figures is consistent to the Fig. 4. For the 6T7D case, frozen-b_{ij}^{Δ} propagation RANS exhibits an overprediction of k in the wake regions (h), indicating the importance of R^{Wake} in wake interactions. The overprediction increases sequentially after each turbine, similar to the baseline RANS (j). This behavior is also observed in the model-b_{ij}^{Δ} RANS (i). However, neither the LES data (f) nor the full propagation RANS (g) exhibit this behavior noticeably. Regarding the U_x, model-b_{ij}^{Δ} RANS (d) closely match the frozen-b_{ij}^{Δ} propagation RANS (c). In the model-b_{ij}^{Δ} RANS, due to the overprediction of k, the wake recovery is slightly faster compared to frozen-b_{ij}^{Δ} propagation RANS, but significantly slower than that of the baseline RANS (e), in which k is significantly overpredicted (j).

In conclusion, the visual assessment above suggests that the obtained model could be effectively implemented in RANS simulations, demonstrating relatively good accuracy. In the following subsection, its ability to predict power production is assessed.

3.3. Power output prediction

In this section, we conduct power output predictions for various simulations. The Figure 6 presents a comparison of each turbine's power output, normalized to the first turbine's power output in the LES data. The full propagation RANS closely match the LES data across the domain. The baseline RANS overestimates for the downstream turbines, particularly for the second one. This is likely due to faster wake recovery, as power is proportional to the cube of the incoming velocity, making the accuracy of U_x crucial for correct power output prediction.

Comparing the full and frozen-b_{ij}^{Δ} propagation RANS, it's observed that the inclusion of the R^{Wake} correction has very small impact on the power output prediction accuracy. However, this doesn't necessarily imply that R^{Wake} is unimportant. The omission of this term in this study

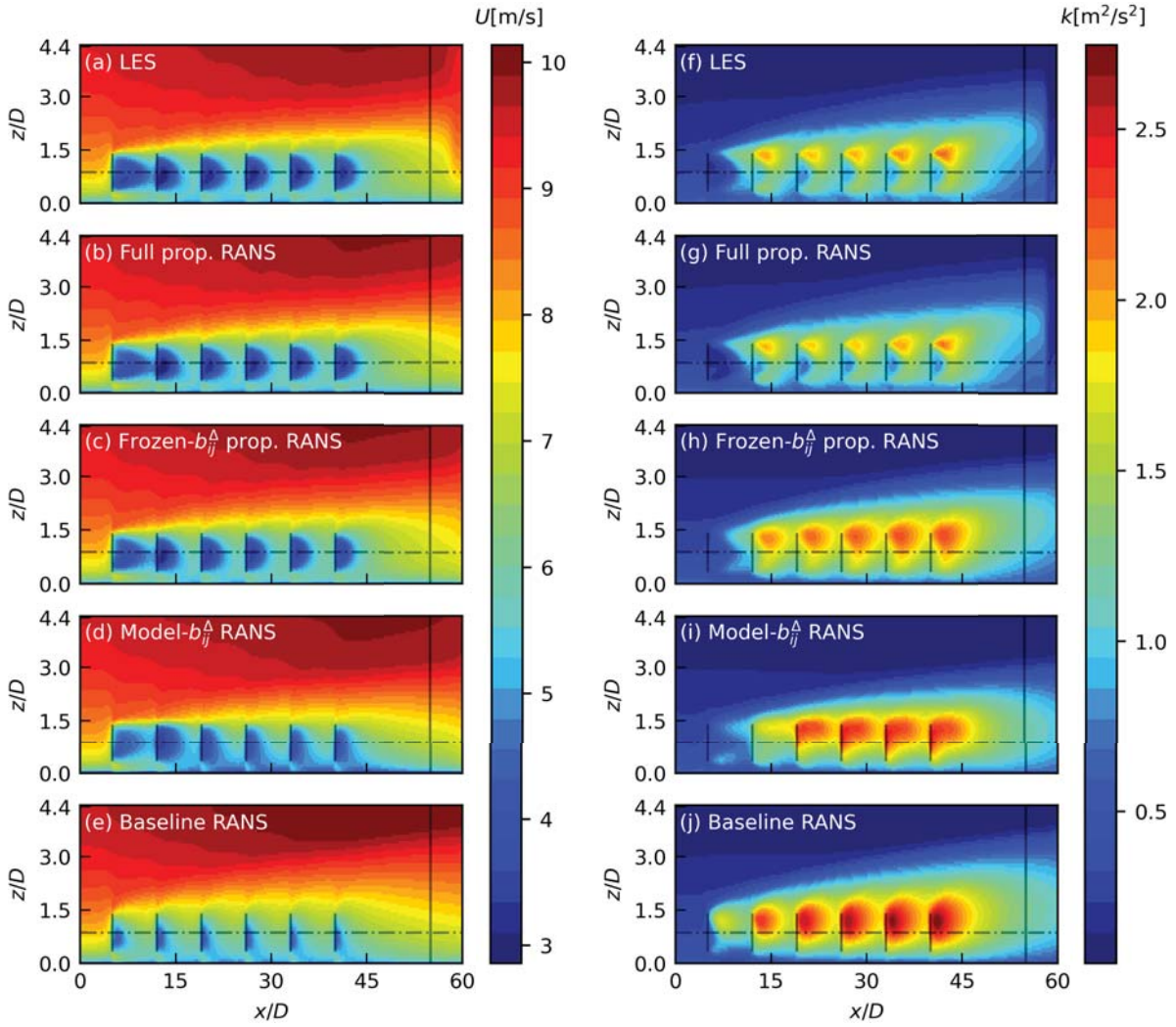

Figure 5: Comparison of $x-z$ planes of U_x (left column) and k (right column) fields at $y = 2.5D$ for 6T7D case simulations. Top to bottom, LES (a, f), full propagation RANS (b, g), frozen-b_{ij}^{Δ} propagation RANS (c, h), model-b_{ij}^{Δ} RANS (d, i), and baseline RANS (e, j) fields are shown, respectively. Dark rectangles represent the ADs, and dash-dotted lines indicate the hub heights.

was for the model simplicity, and its effect is small at least for the cases studied here. Further investigation is required with different simulation cases to explore the impact of R^{Wake}.

The prediction of the model-b_{ij}^{Δ} RANS closely align with the frozen-b_{ij}^{Δ} propagation RANS, despite only being trained with 1T case. This suggests that, at least for this simulation setup, the physics present in the single turbine case may still dominate in multiple turbine scenarios.

4. Conclusion

The primary focus of this study is to develop a simple model for correcting the deviatoric part of the RST using the SpaRTA framework. The training dataset consists of LES data of a single turbine, and a sample pre-selection process is employed to enhance the efficiency of the model discovery process within the framework. The outcome of this study is a simple model for the correction term of the deviatoric part of the RST.

The model consists of two terms, that are made up from the first tensor and the first

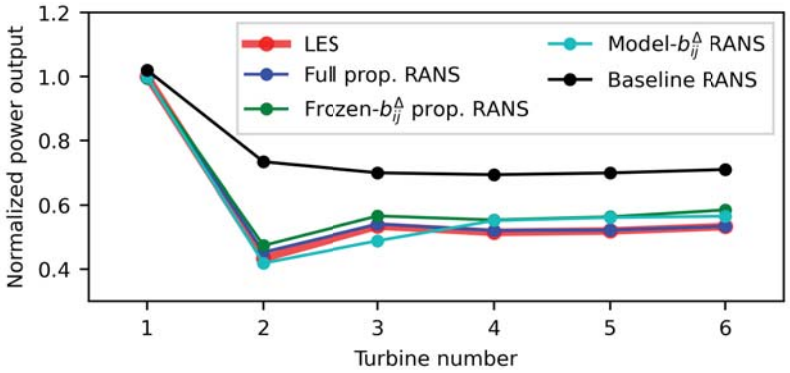

Figure 6: Comparisons of power output for different models. The power output is normalized with respect to the power output of the first turbine in the LES data.

invariant of the Pope's basis tensors, along with the specific dissipation rate that is used for non-dimensionalization. The model works as an modification to the constant C_μ, thus making the model in the scope of the linear eddy viscosity model. The model could capture velocity fields relatively well, but slightly deviates for the TKE field for the trained data. Additionally, when applied to a more complex six-turbine unseen case, the model demonstrates consistent performance in terms of velocity field and power output prediction, except for the TKE field, highlighting its generalizability.

In future research, it is recommended to consider using different baseline models for minimal corrections and improved model comparisons. Additionally, a thorough investigation into the computational costs associated with the modeling approach is necessary, to justify its utilization. In addition to that, to attain the accuracy of full propagation RANS, it is necessary to conduct a discovery of the R^{Wake} model. Furthermore, it is essential to assess the models' generalizability by testing them against more complex scenarios, such as configurations with turbines placed closer together or in staggered arrangements.

Acknowledgments

The authors would like to express appreciation to Dr. Mahdi Abkar for sharing the LES data and to the reviewers for their comprehensive comments.

References

[1] Barthelmie R, Hansen K S, Frandsen S, Rathmann O, Schepers J, Schlez W, Phillips J, Rados K, Zervos A, Politis E and Chaviaropoulos P 2009 *Wind Energy* **12** 431 – 444
[2] Réthoré P 2009 *Wind Turbine Wake in Atmospheric Turbulence* Ph.D. thesis
[3] Archer C L, Vasel-Be-Hagh A, Yan C, Wu S, Pan Y, Brodie J F and Maguire A E 2018 *Applied Energy* **226** 1187–1207
[4] Porté-Agel F, Bastankhah M and Shamsoddin S 2019 *Boundary-Layer Meteorology* **174** 1 – 59
[5] Eidi A, Ghiassi R, Yang X and Abkar M 2021 *Renewable Energy* **179** 2212–2223
[6] Schmelzer M, Dwight R P and Cinnella P 2019 *Flow, Turbulence and Combustion* **104** 579–603
[7] Steiner J, Dwight R P and Viré A 2022 *Computers & Fluids* **233** 105213
[8] Huijing J P, Dwight R P and Schmelzer M 2021 *Computers & Fluids* **225** 104997
[9] van der Laan M P 2014 *Efficient Turbulence Modeling for CFD Wake Simulations* Ph.D. thesis Denmark
[10] Pope S B 1975 *Journal of Fluid Mechanics* **72** 331 – 340
[11] Nelder J A and Mead R 1965 *The Computer Journal* **7** 308–313
[12] Abkar M and Porté-Agel F 2015 *Journal of Renewable and Sustainable Energy* **7** 013121
[13] Calaf M, Meneveau C and Meyers J 2010 *Physics of Fluids* **22** 015110
[14] Launder B and Spalding D 1974 *Computer Methods in Applied Mechanics and Engineering* **3** 269–289
[15] van der Laan M P, Sørensen N N, Réthoré P E, Mann J, Kelly M C, Troldborg N, Schepers J G and Machefaux E 2015 *Wind Energy* **18** 889–907